Catalysis Today 179 (2012) 149–158

Contents lists available at SciVerse ScienceDirect

Catalysis Today

journal homepage: www.elsevier.com/locate/cattod

Study of vanadium based mesoporous silicas for oxidative dehydrogenation of propane and *n*-butane

Roman Bulánek[a,*], Alena Kalužová[a,1], Michal Setnička[a,1], Arnošt Zukal[b,2], Pavel Čičmanec[a,1], Jana Mayerová[b,2]

[a] Department of Physical Chemistry, University of Pardubice, Studentská 573, CZ532 10 Pardubice, Czech Republic
[b] J. Heyrovsky Institute of Physical Chemistry Academic of Sciences of the Czech Republic, v.v.i., Dolejškova 2155/3, CZ182 23 Prague 8, Czech Republic

ARTICLE INFO

Article history:
Received 15 April 2011
Received in revised form 18 August 2011
Accepted 29 August 2011
Available online 25 September 2011

Keywords:
Vanadium
Oxidative dehydrogenation
Mesoporous silicas
Propene
Butenes

ABSTRACT

The comparative study of catalytic performance of V-containing high-surface mesoporous siliceous materials (HMS, SBA-16, SBA-15 and MCM-48) in oxidative dehydrogenation of propane and *n*-butane (C_3-ODH and C_4-ODH, respectively) was carried out. The aim of study was to investigate effect of silica support texture on the speciation of vanadium complexes and its impact on catalytic behavior in both above mentioned reactions is reported. Prepared catalysts were characterized by XRF for determination of vanadium content, XRD, SEM and N_2-adsorption for study of morphology and texture, and H_2-TPR and DR UV–vis spectroscopy for determination of vanadium complex speciation. All prepared materials were tested in propane and *n*-butane ODH reaction at 540 °C and obtained catalytic results were correlated with their structural and surface characteristics. On the basis of obtained data we conclude that the structure of mesoporous silica support plays decisive role in the case of application of catalysts in *n*-butane ODH reaction, whereas catalytic performance of investigated catalysts in propane ODH reaction is comparable for all investigated structures. Catalytic performance of investigated materials in C_3-ODH and C_4-ODH can be correlated with population of all tetrahedrally coordinated VO_x complexes and only isolated monomeric VO_x complexes, respectively.

1. Introduction

Main task of today's chemical industry is a production of a large amount of organic compounds. Presently it is very important to find alternative processes for production of these compounds from more economically convenient raw materials and with smaller impact to environment. As an example, we can use alkanes instead alkenes because alkanes are cheaper compared with alkenes (e.g. actual price of propane is 860 € per ton, while price of propene is 1105 € per ton [1]) and they are easily available. Oxidative dehydrogenation (ODH) of alkanes provides a thermodynamically accessible route to the synthesis of alkenes from alkanes. A large number of reviews dealing with the ODH of light alkanes have been published since early 1990s [2–8]. A general feature of the most catalytic systems in ODH is that the selectivity to alkenes decreases with the increasing alkane conversion. In order to avoid the over-oxidation of the primary product of alkane activation, it is necessary to develop highly structured materials with known and controlled speciation of active components. Many catalysts investigated in the ODH reaction are based on the vanadium oxides as the main component [8–30]. Bulky vanadium pentoxide, in fact, is not a good catalytic system for the selective oxidation of alkanes, but spreading the oxide on the quasi-inert matrix such as a support with the formation of centers with peculiar chemical–physical features and reactivity, leads to selective catalytic systems. The vanadium oxides supported on surface of micro- or mesoporous materials attract great interest of scientific community due to the ability to combine unique textural and acid–base properties of support with the redox properties of vanadium oxide species which opens the new possibility to activate alkanes at relatively low temperatures.

Considerable attention has been devoted to investigation of effect of micro- and mesoporous support texture on the oxidative dehydrogenation of propane (e.g. silicalite [31,32], MCM-41 [12,14,18,33–35], SBA-15 [17,34–36], MCF [34,37] and HMS [16,23,34,35]), but only few papers deal with ODH of butane over VO_x-mesoporous support of SBA-15 type [25,38,39]. Some authors rated as best support for vanadia for ODH of propane SBA-15 [17,40,41], while others denoted HMS and MCM-41 [34] as the best support. However, it must be noted, that differences were not

* Corresponding author. Tel.: +420 46 603 75 11; fax: +420 46 603 70 68.
E-mail addresses: roman.bulanek@upce.cz (R. Bulánek), jana.mayerova@jh-inst.cas.cz (J. Mayerová).
[1] Tel.: +420 46 603 75 11; fax: +420 46 603 70 68.
[2] Tel.: +420 26 605 30 55; fax: +420 28 658 23 07.

0920-5861/$ – see front matter © 2011 Elsevier B.V. All rights reserved.
doi:10.1016/j.cattod.2011.08.044

significant and direct comparison of data from various studies is very complicated due to different conditions applied to the catalytic tests by various research groups. More significant differences in the catalytic behavior could be expected in the case of *n*-butane ODH due to higher sensitivity of this reaction to the population of various types of VO_x species, as was very recently reported [42]. However, according to the best of our knowledge, such study was not published in the literature yet. Therefore, we report comparison of catalytic performance of V-containing high-surface siliceous materials of HMS, SBA-15, SBA-16 and MCM-48 structure in ODH of propane and *n*-butane in order to investigate effect of silica support texture on the speciation of vanadium complexes and its impact on catalytic behavior in both above mentioned reactions. Prepared catalysts were characterized by XRF for determination of vanadium content, XRD, SEM and N_2-adsorption for study of morphology and texture, and H_2-TPR and DR UV–vis spectroscopy for determination of vanadium complex speciation. All prepared materials were tested in propane and *n*-butane ODH reaction at 540 °C and obtained catalytic results were correlated with their structural and surface characteristics. On the basis of obtained data we conclude that structure of mesoporous silica support play decisive role in the case of application of catalysts to *n*-butane ODH, whereas catalytic performance of investigated catalysts in propane ODH reaction is comparable for all investigated structures.

2. Experimental

2.1. Catalyst preparation

HMS was prepared according to procedure reported by Tanev and Pinnavaia [43]. 13.6 g of dodecylamine (DDA, Aldrich) was dissolved in the mixture of 225 cm^3 ethanol and 200 cm^3 double-distilled H_2O. After stirring for 20 min, 56 cm^3 of tetraethyl orthosilicate (TEOS, Aldrich) was added dropwise and intensively stirred. The reaction was performed at 25 °C for 18 h under stirring. The solid product was filtered and then repeatedly suspended in 500 cm^3 ethanol and stirred at 25 °C for 1 h in order to remove major part of DDA from obtained solid. Finally, the solid was calcined in flow of air at 540 °C for 8 h with heating rate 1 °C min^{-1}.

MCM-48 samples were prepared using a mixture of triblock copolymer Pluronic P123 (Aldrich) and *n*-butanol (Aldrich, 99.4%) as a structure-directing mixture and TEOS as the silica source [44]. In the typical synthesis 20 g of Pluronic P123 and 33.5 cm^3 of hydrochloric acid (37%) are dissolved in 720 cm^3 of distilled water to form a clear solution. Then 24.66 cm^3 of *n*-butanol was added; afterwards the mixture was being stirred at 35 °C for 3 h. It was followed by addition of 46.1 cm^3 of TEOS and stirring at 35 °C for 2 h. The reaction mixture was afterwards aged without any stirring for 24 h at 35 °C and 24 h at 95 °C. The resulting solid phase was recovered by hot filtration, extensively washed out with distilled water and dried at 95 °C in Büchner funnel overnight. Calcination was carried out in air at 540 °C for 8 h with heating rate 1 °C min^{-1}.

Purely siliceous SBA-15 mesoporous molecular sieve were synthesized as reported earlier [45] using a triblock copolymer, Pluronic P123 ($EO_{20}PO_{70}EO_{20}$, BASF/Aldrich) as a structure directing agent. TEOS was used as a silica precursor yielding a typical synthesis molar ratio TEOS:HCl:P123:H_2O = 1:6.2:0.017:197. The synthesis mixture was vigorously stirred at 35 °C for 5 min and subsequently aged under static conditions for 24 h at 35 °C and 48 h at 97 °C. The resulting solid was recovered by filtration, extensively washed out with distilled water and ethanol, and dried at 100 °C overnight. The template was removed by calcination in a stream of air at 540 °C for 8 h with heating rate 1 °C min^{-1}.

SBA-16 samples were synthesized using Pluronic P123 and F127 as templates [46]. In the typical synthesis 3.27 g of Pluronic P123, 10.21 g of Pluronic F127 and 91 cm^3 of hydrochloric acid (37%) are dissolved in 550 cm^3 of distilled water to form a clear solution. After that 50 cm^3 of TEOS was added and the mixture was being stirred for 5 min. The reaction mixture was afterwards aged without any stirring for 24 h at 35 °C and 24 h at 95 °C. The resulting solid phase was recovered by hot filtration, extensively washed out with distilled water and dried at 95 °C in Büchner funnel overnight. Calcination was carried out in air at 540 °C for 8 h with heating rate 1 °C min^{-1}.

Vanadium oxo-complexes were doped onto silica support by standard wet impregnation procedure by appropriate amount of ethanol/H_2O solution of vanadyl acetylacetonate (Aldrich). Impregnated samples were dried at 120 °C in air overnight and then calcined at 600 °C for 8 h in the dry air flow. The samples with vanadium loading 3.6 and 9 wt.% were prepared representing materials with vanadium content close to monolayer and markedly exceeding this level. Surface density of vanadium on silica surface at monolayer is usually reported to be 0.7 V/nm^2 [47,48].

2.2. Catalysts characterization

The chemical composition of all investigated samples was determined by X-ray fluorescence spectroscopy by ElvaX (Elvatech, Ukraine) equipped with Pd anode. Samples were measured against the model samples (a mechanical mixture of pure SiO_2 and $NaVO_3$) granulated to the same grain size as catalysts.

The particle morphology of starting mesoporous silicas as well as modified samples was evaluated by scanning electron microscopy images using a JEOL JSM-5500LV instrument.

X-ray powder diffraction data were recorded on a Bruker D8 X-ray powder diffractometer equipped with a graphite monochromator and a position-sensitive detector (Vantec-1) using Cu Kα radiation (at 40 kV and 30 mA) in Bragg–Brentano geometry.

Nitrogen was used as adsorptive and supplied by Messer (Griesheim, Germany – purity 99.999 vol.%). Sorption isotherms of nitrogen at 77 K were determined using an ASAP 2020 instrument. In order to attain a sufficient accuracy in the accumulation of the adsorption data, this instrument is equipped with pressure transducers covering the 133 Pa, 1.33 kPa and 133 kPa ranges. Before each sorption measurement the sample was degassed to allow a slow removal of the most of preadsorbed water at low temperatures. This was done to avoid potential structural damage of the sample due to surface tension effects and hydrothermal alternation. Starting at ambient temperature the sample was degassed at 110 °C (temperature ramp of 0.5 °C min^{-1}) until the residual pressure of 1 Pa was attained. After further heating at 110 °C for 1 h the temperature was increased (temperature ramp of 1 °C min^{-1}) until the temperature of 250 °C was achieved. The sample was degassed at this temperature under turbomolecular pump vacuum for 8 h.

The UV–vis diffuse reflectance spectra of dehydrated diluted samples were measured using Cintra 303 spectrometer (GBC Scientific Equipment, Australia) equipped with a Spectralon-coated integrating sphere using a Spectralon coated discs as a standard. The spectra were recorded in the range of the wavelength 190–850 nm. The samples were diluted by the pure silica (Fumed silica, Aldrich) in the ratio 1:100. All samples were granulated and sieved to fraction of size 0.25–0.5 mm, dehydrated before the spectra measurement and oxidized in the glass apparatus under static oxygen atmosphere in two steps: 120 °C for 30 min and 450 °C for 60 min and subsequently cooled down to 250 °C and evacuated for 30 min. After the evacuation the samples were transferred into the quartz optical cuvette 5 mm thick and sealed under vacuum. For additional details you can see Ref. [49]. This procedure guaranteed complete dehydration and defined oxidation state of vanadium for all catalysts. The obtained reflectance spectra were transformed

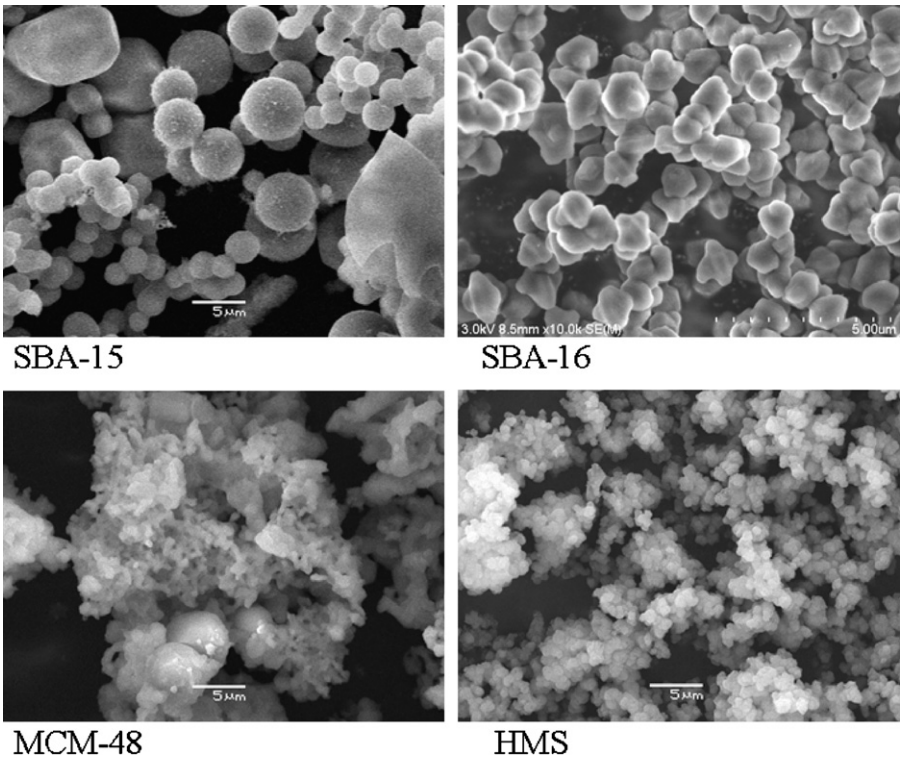

Fig. 1. SEM images of parent mesoporous silicas.

into the dependencies of Kubelka–Munk function $F(R_\infty)$ on the absorption energy $h\nu$ using Eq. (1):

$$F(R_\infty) = \frac{(1-R_\infty)^2}{2R_\infty} \quad (1)$$

where R_∞ is the measured diffuse reflectance from a semi-infinite layer [50].

All measured spectra were simultaneously fitted [49] by set of Gaussian curve shaped bands using the Fityk [51] software. Because all VO_x species exhibit the same or similar absorption coefficients [49] it is possible to make the semi-quantitative analysis of spectra.

Raman spectra of dehydrated catalysts were measured by a Labram HR spectrometer (Horiba Jobin-Yvon) interfaced to an Olympus BX-41 microscope. Spectra were excited by 514.5 nm line of an Ar^+/Kr^+ laser (Innova 70C series, Coherent). The Raman spectrometer was calibrated by using the F_{1g} line of Si at 520.5 cm^{-1}. The spectra were recorded with resolution 2 cm^{-1} by Peltier-cooled CCD camera detector. The laser power impinging on the dry sample was 1.2 mW. The dehydration and oxidation protocol was the same as for DR UV–vis measurement (see above).

Redox behavior of VO_x surface species was investigated by the temperature programmed reduction by hydrogen (H_2-TPR) using the AutoChem 2920 (Micromeritics, USA). 100 mg sample in a quartz U-tube microreactor was oxidized in oxygen flow at 450 °C (2 h) prior to the TPR measurement. The reduction was carried out from 100 °C to 900 °C with a temperature gradient of 10 °C min^{-1} in flow of reducting gas (5 vol.% H_2 in Ar). The changes of hydrogen concentration were monitored by the TCD detector.

2.3. Catalytic tests in ODH reaction

The propane and *n*-butane oxidative dehydrogenation (C_3-ODH and C_4-ODH, respectively) reaction was carried out using a plug-flow fixed-bed reactor at atmospheric pressure in the kinetic region (independently checked) and at steady state conditions of the reaction. The activity and selectivity of catalysts were tested at 540 °C in the dependence on contact time (W/F 0.03, 0.06, 0.09, 0.12 and 0.15 g_{cat} s cm^{-3}). The demanded weight of catalyst (grains 0.25–0.50 mm) was mixed with 2 cm^3 of inert SiC. The catalysts were pre-treated in a flow of oxygen at 540 °C for 2 h before each reaction run. The feed composition was $C_xH_y/O_2/He = 5/2.5/92.5$ vol.% with a total flow of 100 cm^3 min^{-1} STP (C_xH_y – C_3H_8 or C_4H_{10}). The catalytic activity was analyzed at steady state conditions and the products composition was analyzed by on-line gas chromatograph equipped with TCD and FID detectors. The feed conversion, selectivity to products and productivity were calculated based on mass balance according to Sachtler and Boer [52]. The turn-over-frequency (TOF) values per V atom were calculated using Eq. (2):

$$\mathrm{TOF}_X = \frac{n^0_{n-C} X_{n-C} M_V}{m_{cat} w_V} \quad (2)$$

where n^0_{n-C} is molar flow of hydrocarbon (mol s^{-1}), X_{n-C} conversion of hydrocarbon (%), M_V is atomic weight of vanadium (50.94 g mol^{-1}), m_{cat} is weight of catalyst (g), w_v is mass fraction of vanadium in catalysts.

3. Results and discussion

3.1. Physicochemical properties of the samples

SEM images of all four starting materials (Fig. 1) have revealed regular particle morphology without any presence of other phases. For comparison there are shown samples of SBA-15 containing different amounts of vanadium (Fig. 2) and it can be concluded that as far as particle size and morphology is concerned, no effect due to the presence of vanadium was observed.

XRD patterns of parent materials (Fig. 3A) exhibit well resolved diffraction lines, which can be associated with well-ordered pore structure of the mesoporous SBA-15, MCM-48 and SBA-16 as well as the disordered wormhole-like pore structure of HMS. After

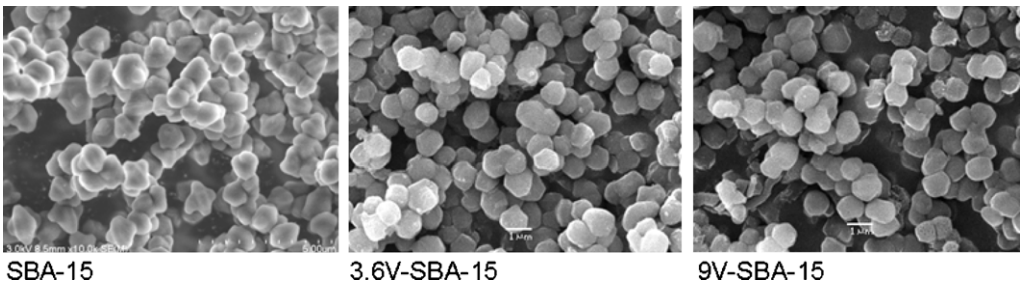

Fig. 2. SEM images of parent SBA-15 and its vanadium modified forms.

impregnation of parent materials with vanadium complex, the same diffraction lines are observed, indicating the preserved ordering of mesoporous structure as demonstrated on 3.6 and 9V-SBA-15 samples (see Fig. 3B). However, substantial decrease of intensity of diffraction lines was observed. The decrease in intensity of the peaks after post-synthesis modifications demonstrates the partial structural collapse of the mesoporous materials or the flexibility induced in the silica framework due to the strain generated from the functionalized groups [53,54].

Nitrogen adsorption isotherms of all starting and impregnated samples of selected silica SBA-15 are illustrated in Fig. 4. It was found that despite rather rough treatment of primary samples the hysteresis loop of impregnated samples remains preserved. It confirms that modification of parent samples did not significantly change the structure of these materials. In addition isotherms are characteristic of high quality of prepared materials. The BET surface area was evaluated using adsorption data in a relative pressure range from 0.05 to 0.25 (Table 1). The micropore volume (V_{MI}) was determined using *t*-plot method. The mesopore volume (V_{ME}) and mesopore distribution of silica materials were calculated using BJH algorithm (Table 1) calibrated to accurately reproduce the pore diameter and volume. In particular, the changes in S_{BET} illustrate a pronounced reduction of the surface (mainly micropore volume) which was accessible for nitrogen molecules due to the vanadium impregnation. Samples doped with the highest concentration of vanadium exhibited decrease of S_{BET} from 60% to 75% related to their parent samples. On the other hand the decrease of mesopore volumes of the same materials was only in the range from 20% to 48%. Introduction of vanadium into mesopores also affected the pore size distribution. This effect is shown on SBA-15 samples (see Fig. 5), where the higher concentration of vanadium, the lower is the peak on the distribution curve. Moreover, the pore size distribution was slightly shifted to lower values of pore diameter.

The diffuse reflectance UV–vis spectroscopy provides information about the character and oxidation state of vanadium. The obtained DR UV–vis spectra for both prepared sets of catalyst are presented in Fig. 6. It can be noted that parent silica supports exhibited only very low intensity spectrum and therefore are not reported here. All spectra were obtained by measurement of one hundred times diluted dehydrated samples with the purpose to obtain better resolution of individual bands and the linear dependence area of spectra on the concentration of vanadium (for more details see Ref. [49]). They are qualitatively similar to spectra published previously for the vanadium oxide system on the different siliceous supports [13,55,56] and contain several absorption bands in region 1.46–6.5 eV (850–190 nm) which are conventionally attributed to ligand to metal charge-transfer (LMCT) transitions of the $O \rightarrow V^{+V}$ type or to the d-d transitions of V^{+IV} [56]. The d–d absorption bands characteristic for the vanadium(+IV) in the region 1.55–2.07 eV [57] were not observed in our obtained spectra and this fact confirms that all vanadium was successfully oxidized to oxidation state (+V) during

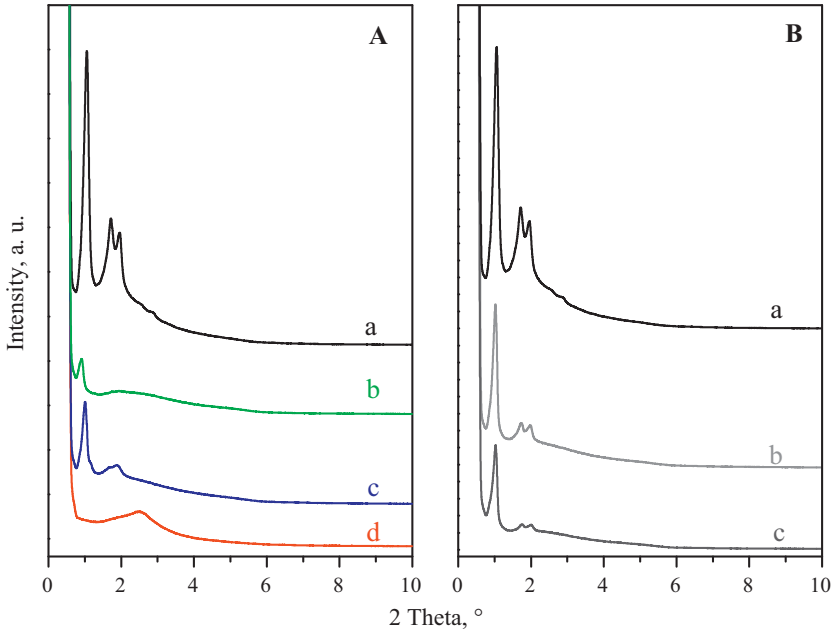

Fig. 3. (A) XRD patterns of parent mesoporous silica supports: (a) SBA-15, (b) SBA-16, (c) MCM-48, (d) HMS. (B) XRD patterns of parent SBA-15 and its vanadium modified forms: (a) SBA-15, (b) 3.6V-SBA-15, (c) 9V-SBA-15.

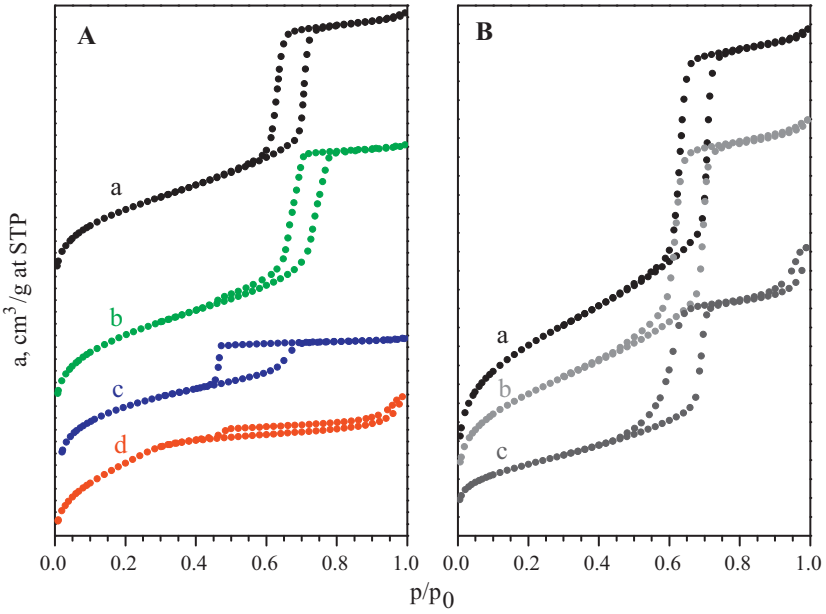

Fig. 4. (A) Nitrogen adsorption isotherms of parent mesoporous silica supports: (a) SBA-15, (b) SBA-16, (c) MCM-48, (d) HMS. (B) Nitrogen adsorption isotherms of parent SBA-15 and its vanadium modified forms: (a) SBA-15, (b) 3.6V-SBA-15, (c) 9V-SBA-15.

the pretreatment procedure. The samples with high concentration of vanadium exhibit absorption bands in the region 2–3 eV with maxima at ca. 2.6 and 3.1 eV and they are attributed to the presence of 3D-octahedrally coordinated (group O_h) bulk-like VO_x units [13,49,57]. The low-loaded samples exhibit absorption only above 3 eV evidencing VO_x species with tetrahedral coordination. Fig. 7 shows spectra of low-loaded samples together with spectra of sodium ortho-vanadate Na_3VO_4 and meta-vanadate $NaVO_3$ as standard compounds containing only isolated monomeric tetrahedral units and linearly polymerized tetrahedrally coordinated oligomeric units with V–O–V bonds respectively. Our samples with lower vanadium content exhibit edge energy 3.7–3.47 eV (obtained accordingly to Ref. [58]), whereas edge energy of Na_3VO_4 and $NaVO_3$ is 3.82 and 3.13 eV, respectively. Taking into account this observation, it is concluded that both isolated VO_4 units and small VO_x aggregates that have V–O–V bonds are present on the surface of our samples (effect of partial hydratation was excluded on the base of checking measurement of overtones of OH group vibration on UV–vis–NIR spectrometer). For quantitative analysis of all three types of surface vanadium complexes, the spectra were deconvoluted into individual bands. Parameters of individual spectral bands used in deconvolution procedure of the spectra were taken from systematic study analyzing set of VO_x–HMS samples with wide range of vanadium concentration and vanadium species distribution recently published [49]. Fig. 8 presents example of the deconvolution of the experimental spectra for the samples with low and high concentration of VO_x species anchored on SBA-15 support. UV–vis spectra of all samples (with low and high concentration) contain three absorption bands in the region 3–6.5 eV and these bands can be attributed to the ligand to metal charge transfers of T_d-coordinated species (group of symmetry T_d). The band with maxima position approximately at 4 eV can be attributed to T_d-oligomeric species [49,59,60]. The band at ca. 5.9 eV belongs to T_d-monomeric species [49,59–61] and the band with maximum at 5 eV is linear combination of the bands ascribed to both the T_d-monomeric and the T_d-oligomeric species. For more information

Table 1
Chemical composition and results of physico-chemical characterization of investigated materials.

Sample name	V[a], wt.%	S_{BET}, $m^2\ g^{-1}$	V_{MI} [b], $cm^3\ g^{-1}$	V_{ME} [c], $cm^3\ g^{-1}$	D_{ME} [d], nm	VO_x [e], nm^{-2}	X_{mono} [f]	X_{oligo} [f]	X_{O_h} [f]	T_{max} [g], °C	Δe[h]
HMS		879	0.010	0.189	6.9						
SBA-15		780	0.060	0.820	6.7						
SBA-16		710	0.073	0.510	3.9						
MCM-48		820	0.068	0.770	7.0						
3.6V-HMS	3.6	640	0.025	0.176	7.1	0.7	0.42	0.58	0	568	1.5
3.6V-SBA-15	3.6	600	0.030	0.730	5.6	0.7	0.82	0.18	0	555	1.8
3.6V-SBA-16	3.6	570	0.043	0.309	4.0	0.7	0.56	0.44	0	534	1.6
3.6V-MCM-48	3.6	670	0.045	0.678	6.0	0.6	0.55	0.45	0	562	1.9
9V-HMS	9.0	260	0.039	0.150	8.6	4.0	0.28	0.60	0.12	594	1.6
9V-SBA-15	9.0	300	0.011	0.571	6.1	3.4	0.53	0.43	0.03	572	1.7
9V-SBA-16	9.0	130	0.011	0.228	10.0	8.1	0.47	0.44	0.10	596	1.7
9V-MCM-48	9.0	350	0.018	0.545	7.0	3.1	0.46	0.47	0.07	587	1.6

[a] Vanadium content determined by XRF method.
[b] V_{MI} micropore volume determined by using the *t*-plot method.
[c] V_{ME} mesopore volume determined by Barret–Joyner–Halenda (BJH) algorithm.
[d] D_{ME} mesopore diameter determined by BJH algorithm.
[e] VO_x surface density ($VO_x\ nm^{-2}$).
[f] Relative amount of T_d-monomeric, T_d-oligomeric and O_h units.
[g] Position of maxima of H_2-TPR profile.
[h] Average change of oxidation state during H_2-TPR experiment.

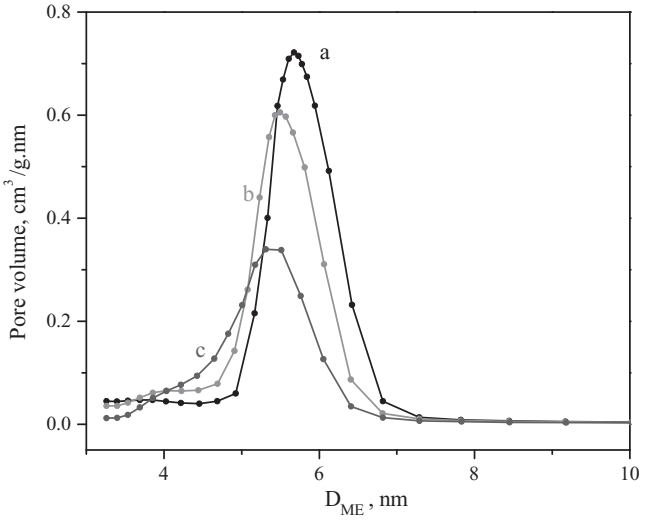

Fig. 5. Pore size distribution for parent SBA-15 and its vanadium modified forms: (a) SBA-15, (b) 3.6V-SBA-15, (c) 9V-SBA-15.

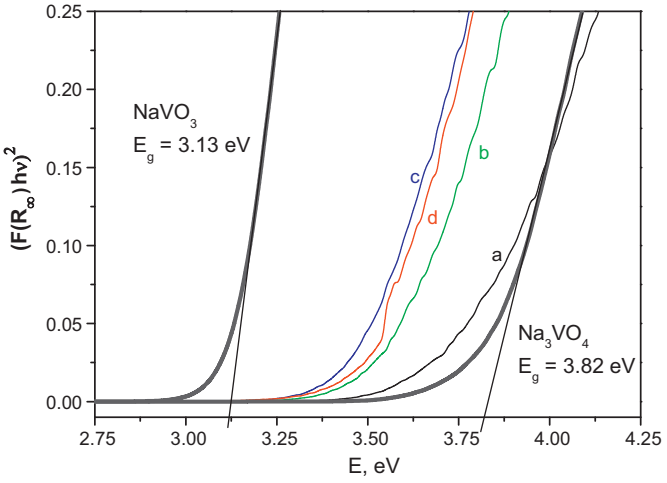

Fig. 7. Diffuse reflectance UV–vis spectra of diluted and dehydrated low-loaded VO_x catalysts (colors are the same as in Fig. 6A), ortho- and meta-vanadate with corresponding edge of absorption energy. (a) SBA-15, (b) SBA-16, (c) MCM-48, (d) HMS.

about assignment see Ref. [49]. Relative amount of individual VO_x species on the surface was determined from area of corresponding bands and results are given in Table 1. The low concentrated samples contain only T_d-coordinated VO_x species with predominantly T_d-monomeric units which are considered to be the most active particles in the light alkane ODH reactions [5,62]. The highest relative abundance of monomeric T_d-coordinated units can be found on the SBA-15 support, approximately about 85% relative amount for lower concentration of vanadium. For other low concentrated samples the amounts of monomeric units are significantly lower (about 50%). On the basis of the supports tendency to generate the T_d-oligomeric and octahedrally coordinated polymeric units we can sort tested support materials in the following order SBA-15 < SBA-16 ~ MCM-48 < HMS. We can observe this influence in samples with high concentration as well (see Table 1). High capability of SBA-15 for accommodation of well dispersed isolated monomeric vanadyl species can be given by the fact that SBA-15 silica represents mesoporous support with regular, well defined and uniform pore system characterized by very narrow pore size distribution, whereas other investigated supports exhibit worm-like (HMS) or ink-bottle (MCM-48) type of pores with wider distribution of pore diameters, which are less suitable for fine dispersion of source of vanadium during the procedure of solvent evaporation. The more regular pore system the more homogeneously is solvent removed from inner space of pore system. The Raman spectra of the dehydrated VO_x catalysts are shown in Fig. 9 (part A of Fig. 9 shows the spectra of low-loaded samples, part B of Fig. 9 shows the spectra of high-loaded samples). The catalysts possess Raman features at 282, 301, 404, ~487, 520, 697, ~802, 993 and 1031 cm^{-1}. The

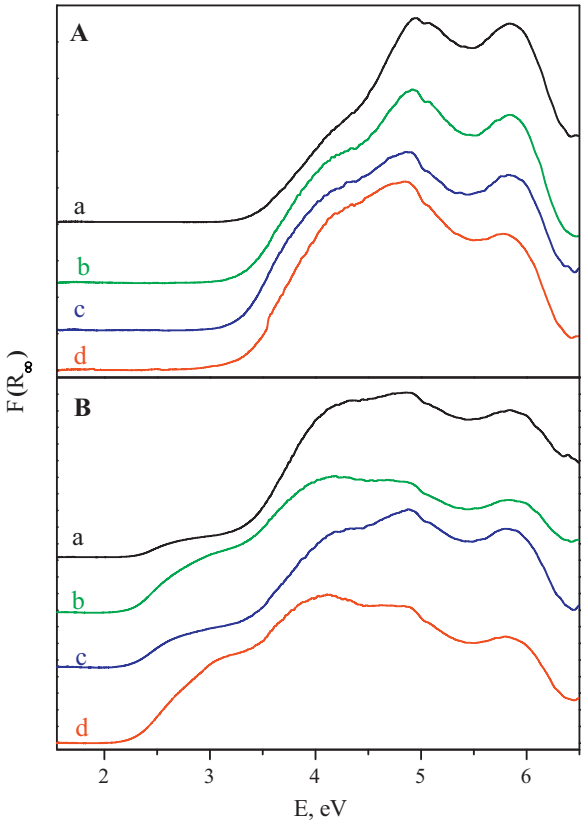

Fig. 6. Diffuse reflectance UV–vis spectra of diluted and dehydrated VO_x catalysts on different support with 3.6 (A) and 9 (B) wt.% of V: (a) SBA-15, (b) SBA-16, (c) MCM-48, (d) HMS.

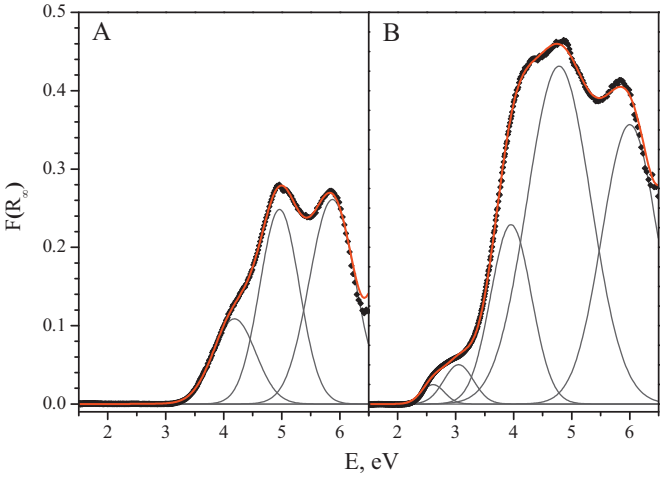

Fig. 8. Deconvoluted UV–vis spectra of V-SBA-15 with (A) 3.6 and (B) 9 wt.% of V. Black points are experimental data, red line is fitted envelope curve and dark gray lines are individual spectral bands. (For interpretation of the references to color in this figure legend, the reader is referred to the web version of this article.)

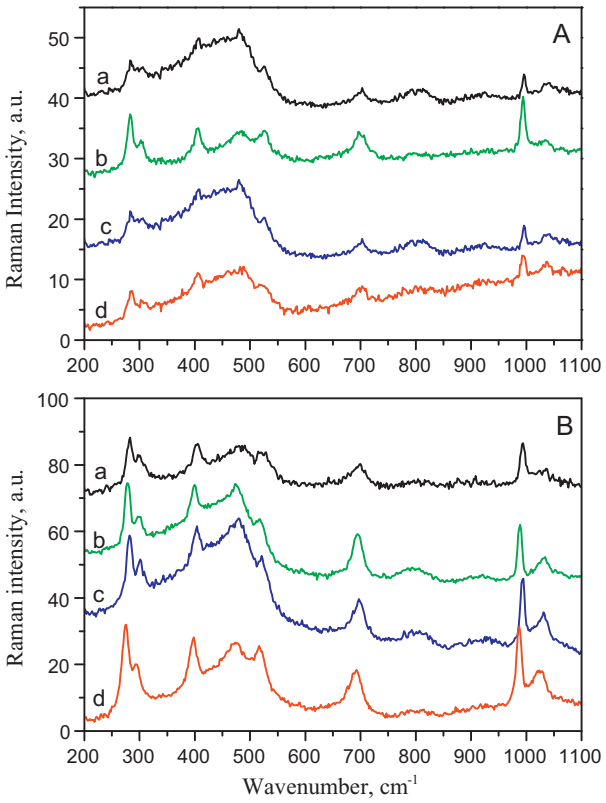

Fig. 9. Raman spectra of the dehydrated VO_x–silica samples with 3.6 (A) and 9 (B) wt.% of V: (a) SBA-15, (b) SBA-16, (c) MCM-48, (d) HMS.

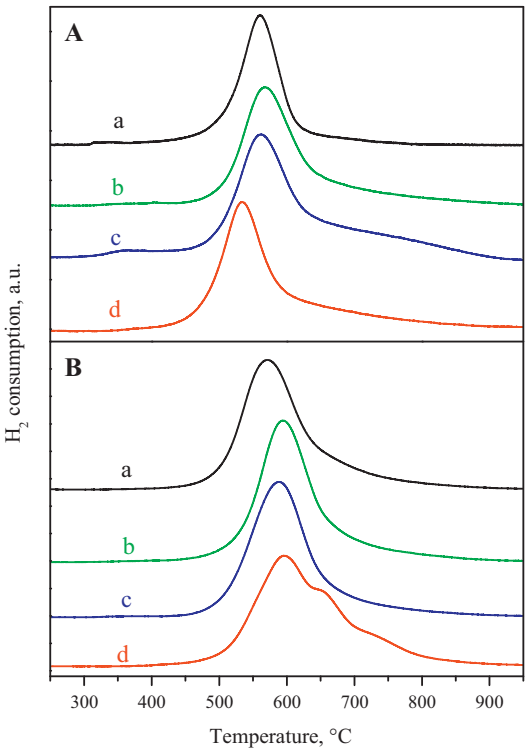

Fig. 10. H_2-TPR patterns of VO_x–silica samples with 3.6 (A) and 9 (B) wt.% of V: (a) SBA-15, (b) SBA-16, (c) MCM-48, (d) HMS.

bands at ~802 and ~487 cm^{-1} have been assigned to the symmetrical Si–O–Si stretching mode and the D1 defect mode of silica support, which have been attributed to tetracyclosiloxane rings produced via the condensation of surface hydroxyls [63,64]. All other bands can be attributed to vibration connected with presence vanadium species. It has been generally agreed that Raman bands in the range 800–1200 cm^{-1} are due to stretching modes and the bands below 800 cm^{-1} are due to bending/stretching modes of V–O [65,66]. Assignment of the Raman band is complicated by strong coupling of vanadyl stretching and silica modes, which are close in vibration energy [66,67]. However, band at 1031 cm^{-1} is usually assigned to terminal V=O stretching vibration. Shift of this vibration band to slightly higher wavenumbers was frequently taken as evidence of changes in the coordination and extent of polymerization of the dehydrated surface VO_x species on oxide supports as Al_2O_3, ZrO_2, TiO_2 or Nb_2O_5 [47,68]. However, no shift of this Raman band was observed on VO_x/SiO_2 systems [47,68,69]. This is in agreement with our observations. Position of this band is invariable notwithstanding various population of oligomeric species determined from UV–vis spectra. Recent theoretical and experimental papers dealing with vibration of vanadium species on silica surface confirmed that both monomeric and oligomeric vanadium complexes contribute to this band [59,66,67,70]. Above mentioned strong coupling of VO_x species vibration with silica skeletal vibration could be behind observed no shift of this band with progressive polymerization of VO_x species. Set of bands at 282, 301, 404, 520, 697, and 993 cm^{-1} are ascribed to V_2O_5 crystallites. It is interesting to note that above mentioned bands are present in all Raman spectra while typical bands assigned to V_2O_5 crystallites at 2.6 and 3.1 eV are detected only in DR UV–vis spectra of samples with 9 wt.% of vanadium (cf. Fig. 6). Therefore, Raman spectra prove the presence of very small amount of V_2O_5 crystallites, which cannot be detected by UV–vis spectroscopy or XRD, even in the low-loaded samples due to resonant enhance effect.

H_2-TPR curves of VO_x catalysts are depicted in Fig. 10. It can be noted that parent silica supports exhibited no reduction peaks and therefore are not reported here for the sake of brevity. Vanadium catalysts exhibit distinct reduction peaks in the temperature range from 350 to 900 °C. The average change of oxidation state (Δe) after the H_2 reduction has been calculated from the amount of H_2 consumed during the reduction process and range from 1.5 to 1.9 (see Table 1) indicating incomplete reduction of V^{+V} to V^{+III} or the presence of vanadium cations in lower oxidation states (V^{+IV} or even V^{+III}) in the samples already before starting the TPR process. The reduction peak centered at ca. 534–568 °C dominates the TPR patterns of all investigated materials. This peak is distinctly tailed on high-temperature side for samples with higher vanadium loading, especially for SBA-16 support with 9 wt.% of vanadium. Existence of other peaks at about 650 and 735 °C indicates, in accord with spectroscopic results, certain heterogeneity of vanadium complexes on the inner surface of the prepared catalysts. In previous studies reported in the literature, the low-temperature peak was tentatively attributed to the reduction of highly dispersed VO_x units with tetrahedral-like coordination [12,71–73] and the high-temperature peaks were attributed to the reduction of polymeric oxide-like VO_x species with octahedral coordination [74–78]. We reported in recent study on VO_x-HMS catalysts that presence of high-temperature reduction peak in the H_2-TPR curves of VO_x-HMS catalysts exhibited materials with presence of UV–vis bands at 2.6 and 3.1 eV in their UV–vis spectra ascribed to 2D-square pyramidal and 3D-octahedrally coordinated vanadium species [42]. Therefore, the low-temperature reduction peak could be attributed to both monomeric and oligomeric tetrahedral-like coordinated VO_x species. Generally, reducibility of bulk vanadium oxides differs from reducibility of surface species. Based on comparison of H_2-TPR and ^{51}V NMR characterization of VO_x–SiO_2 materials with various vanadium loading it was concluded that the reduction of bulk V_2O_5

Table 2
Results of catalytic tests in oxidative dehydrogenation of propane at 540 °C and iso-conversion of propane 13% (C_3H_8/O_2/He = 5/2.5/92.5 vol.%, total flow rate of 100 cm^3 min^{-1}).

Catalyst sample name	Conv., %	Selectivity, %				Productivity[b]	TOF, h^{-1}
	O_2	C_3H_6	C_1–C_2 [a]	CO	CO_2	C_3H_6	
3.6V-HMS	65	56	1	26	17	0.22	10
3.6V-SBA-15	59	60	3	23	14	0.21	12
3.6V-SBA-16	61	57	2	26	15	0.21	12
3.6V-MCM-48	63	56	2	26	16	0.17	13
9V-HMS	74	41	0	44	15	0.23	7
9V-SBA-15	62	48	0	38	14	0.38	13
9V-SBA-16	49	50	1	35	14	0.24	6
9V-MCM-48	75	44	0	42	14	0.36	11

[a] C_1–C_2 = sum of C_1–C_2 hydrocarbons.
[b] Productivity = g_{prod} g_{cat}^{-1} h^{-1}.

occurred at much higher temperatures than silica supported vanadia due to increased diffusional limitations in bulk V_2O_5 [75]. On the other hand, Banares et al. observed by in situ TPR-Raman experiments formation of oxide species during heating and reduction of these species at lower temperatures than reduction of monomeric species. In addition, reducibility of individual types of vanadia species can vary in dependence on the support as was experimentally observed by systematic shifts of reduction peak position on temperature scale [78–81]. On VO_x-MCM-41 silica, investigation of reduction kinetics of surface vanadia species in hydrogen atmosphere by means of in situ UV–vis spectroscopy led to conclusion that tetrahedrally coordinated polymeric vanadia species are more reducible than monomeric species [82] similarly to VO_x–Al_2O_3 system [81]. However, position of reduction peak in our TPR curves of low-loaded samples changes within interval of 30 °C, but irrespective to population of monomeric species. Reduction of high-loaded samples is shifted by about 30 °C to higher temperature. This could be caused by increase in population of polymeric species. However, the shift of reduction peak can be influenced not only by nature of species but also by thermodynamics or kinetics limitations (e.g. changes in hydrogen and water concentration in the reduction gas owing the reduction reaction course). Therefore, it is very difficult to attribute a particular surface structure to the individual TPR peaks more reliably.

3.2. Catalytic tests of propane and n-butane ODH

Oxidative dehydrogenation of propane over investigated samples was studied at 540 °C at various contact times realized by changes of catalyst weight. Main results are presented in Table 2. The main products of C_3-ODH were propene and carbon oxides. Traces of ethene and methane were detected as cracking products. No oxygenates were detected. It is well-known that the selectivity is necessary to compare at the same degree of conversion for parallel-consecutive reaction, such as the C_3-ODH reaction. Therefore the catalytic behavior of VO_x–silica catalysts with different vanadium loading and different texture of support was compared under iso-conversion conditions at propane conversion of 13%. In addition, catalytic performance of the samples only slightly depended on time-on-stream (decline of propane conversion and propene selectivity was 1 and 2%, respectively, within 4 h in the stream). Therefore, data after 2 h in the stream were taken for catalysts comparison. The iso-conversion selectivity to propene only slightly varied in the range from 60 to 56% for lower vanadium content regardless of catalysts structure, whereas it reached only 41–50% for materials with higher vanadium loading (see Table 2). The decrease in propene selectivity was accompanied by increase in selectivity to CO. The selectivity to CO_2 was relatively constant and comparable for all catalysts ($S_{CO_2} = 15 \pm 2\%$). The activity of VO_x–silica catalysts under these conditions was expressed by so called turn-over-frequency (TOF), describing the average number of catalytic cycles at one average vanadium atom per time unit (h). The TOF factor was almost constant for catalysts with lower vanadium content (TOF equal to 12 h^{-1} except VO_x-HMS exhibiting TOF of 10 h^{-1}). The TOF for catalysts with higher loading of vanadium depended on type of mesoporous silica support. The VO_x-SBA-15 and VO_x-MCM-48 catalysts exhibited catalytic activity similar to low-vanadium ones (13 and 11 h^{-1} for SBA-15 and MCM-48, respectively), the HMS and SBA-16 supports exhibited TOF values significantly lower (7 and 6 h^{-1} for HMS and SBA-16, respectively). It must be noted that conversion of oxygen did not exceed 75% in any case and therefore both selectivity to product and activity of catalysts were not influenced by lack of reactant. Significantly lower values of TOF of 9V-SBA-16 and 9V-HMS samples corresponded very well with the enhanced population of octahedral VO_x complexes in these samples evaluated by means of deconvolution of UV–vis spectra (cf. Table 1 and Fig. 6).

Oxidative dehydrogenation of *n*-butane was studied at 540 °C at various contact times implemented by changes of catalyst weight. The main reaction products identified in the reaction mixture were: 1-butene (1-C_4), *cis*- and *trans*-2-butene (*c*-C_4 and *t*-C_4), 1,3-butadiene (1,3-C_4), methane (C_1), ethane and ethene (C_2), propane and propene (C_3), carbon oxides (CO and CO_2) and traces of acetaldehyde. The carbon balance was 98 ± 3% in all the catalytic tests and no coke deposit was observed on the catalysts. The activity of catalysts only slightly depended on the time-on-stream (TOS). Average decline of *n*-butane conversion was about 2% within 10 h in the stream. On the other hand this decrease of conversion was accompanied by the increase of C_4-ODH selectivity approximately about 4%. This small change in catalyst performance can be explained by partial redistribution of vanadium oxide species under reaction conditions [56]. Therefore the catalytic performance of VO_x-catalyst on different support and with different vanadium loading was compared under the iso-conversion conditions at *n*-butane conversion of 13% after 2 h in the stream of reaction mixture.

The TOF value strongly depended on the concentration of vanadium and decreased with the increasing VO_x concentration (for the samples with 9 wt.% of V was only 30–40% of the value obtained for samples with 3.6 wt.% V). It can be explained with higher amount of Td-oligomeric and mainly octahedral units on the support (cf. data in Tables 1 and 3, see also Figs. 6 and 8). The value of the TOF was in good agreement with relative concentration of monomeric VO_x units as it is shown in Table 1 and Fig. 11 shows TOF value of low-loaded catalysts as a function of population of monomeric VO_x units and reaction type (C_4- and C_3-ODH). The TOF values of catalysts in C_4-ODH linearly decreased with decreasing relative population of T_d monomers obtained from UV–vis spectra deconvolution, whereas TOF values obtained in C_3-ODH were rather constant irrespective of ratio between amount of T_d monomeric and T_d oligomeric species. Considering this relation the monomeric VO_x units should be taken as the most active species in the ODH of

Table 3
Results of catalytic tests in oxidative dehydrogenation of *n*-butane at 540 °C and iso-conversion of *n*-butane 13% ($C_4H_{10}/O_2/He = 5/2.5/92.5$ vol.%, total flow rate of 100 $cm^3\ min^{-1}$).

Catalyst sample name	Conv., %	Selectivity, %								Productivity[c]	TOF, h^{-1}
	O_2	1-C_4	*c*-C_4	*t*-C_4	1,3-C_4	C_1–C_3 [a]	CO	CO_2	Dehy.[b]	Dehy.[b]	
3.6V-HMS	70	23	10	12	8	5	24	19	53	0.32	16
3.6V-SBA-15	63	23	12	12	12	6	18	15	58	0.57	26
3.6V-SBA-16	63	22	11	14	11	5	20	18	58	0.41	19
3.6V-MCM-48	81	19	8	10	7	4	30	23	43	0.31	19
9V-HMS	95	11	8	10	6	3	42	22	34	0.16	5
9V-SBA-15	95	11	7	9	7	3	39	25	34	0.37	11
9V-SBA-16	87	14	7	9	5	3	37	25	35	0.16	5
9V-MCM-48	97	9	7	9	6	3	40	25	31	0.23	8

[a] C_1–C_3 = sum of C_1–C_3 hydrocarbons and acetaldehyde.
[b] Dehy. = sum of C_4 alkenes.
[c] Productivity = $g_{prod}\ g_{cat}^{-1}\ h^{-1}$.

n-butane, while both monomeric and oligomeric species with T_d coordination could act as active species in ODH of propane.

The iso-conversion selectivity to C_4-ODH is given in Table 3. They were almost independent on the structure of siliceous supports (except 3.6V-MCM-48 exhibiting significantly lower selectivity than other catalysts with 3.6 wt.% of vanadium), but they are strongly decreasing from 58% to 34% with the increasing of vanadium loading for samples with 3.6 and 9 wt.%, respectively. The decrease in C_4-ODH selectivity is accompanied by increase in selectivity to carbon oxides, mainly selectivity to CO. This fact can be explained by higher oxygen conversion over high concentrated samples where it was almost 100%. The decrease of selectivity with the increasing of VO_x concentration was most probably due to higher abundance of oligomeric species with T_d- and mainly O_h-coordination. These species contained the V–O–V bridging oxygen atoms and according to the mechanism introduced by Kung [5] the presence of these units allows the formation of alkoxide intermediates which are furthermore oxidized to the products of total oxidation. Butenes selectivity dependence on the structure of support material is not so distinct in contrast to the mentioned different activity (TOF) discussed above and this effect is due to the relatively complex mechanism of ODH of *n*-butane. The main factors affecting the selectivity are the vanadium content, the vanadium surface density, the nature of the support (structure, acidity) and the reactions temperature [11,55]. Acid character of siliceous support (iso-electric point (IEP) is ca. 2) has probably major influence on the selectivity. Increasing acidity of the catalysts extend retention period of reaction intermediate on the surface of catalyst. The alkenes (electron-donating molecules) are more basic than the corresponding alkanes and they interact more strongly with acid support [11]. This effect allows us to explain the occurrence of the consecutive reactions with neighboring VO_x species regardless on type of T_d-coordinated species. The distance of neighboring species can be related to the surface density and it is similar for all structures of support with 3.6 wt.% of vanadium (0.6–0.7 V per nm^2). In the case of high-loaded catalysts is problem more complex due to presence of significant amount of vanadium pentoxide.

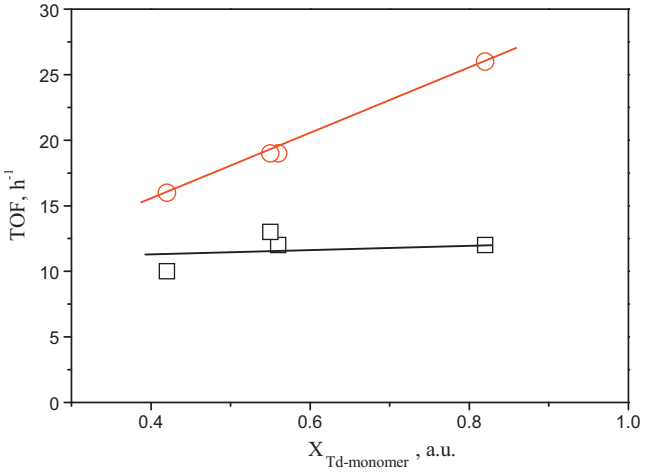

Fig. 11. Dependence of TOF factors of VO_x catalysts with 3.6 wt.% of vanadium on population of monomeric VO_x species determined by deconvolution of DR UV–vis spectra. Red circles – C_4-ODH, black squares – C_3-ODH. (For interpretation of the references to color in this figure legend, the reader is referred to the web version of this article.)

4. Conclusions

The above discussed data allow us to draw the following conclusions:

- Based on H_2-TPR, Raman and DR UV–vis results, it can be concluded that both monomeric and oligomeric species with T_d coordination exist in the all investigated samples. In addition, condensed species with O_h coordination are significantly formed in the samples with vanadium loading of 9 wt.%. Population of individual types of vanadium species is dependent on the type of silica support structure and vanadium content.
- C_3-ODH reaction is sensitive to the presence of condensed species with O_h coordination which caused lowering of catalytic activity and selectivity to propene. Nevertheless, both monomeric and oligomeric tetrahedral species are active and selective in C_3-ODH reaction as is documented by similar iso-conversion selectivity to propene and TOF factors of low-loaded catalysts without condensed VO_x species with O_h coordination, but differing in population of monomeric and oligomeric VO_x species with T_d coordination.
- On the other hand, C_4-ODH reaction is very sensitive to isolation of vanadium species, because monomeric units are much more active and selective than all other species as can be documented by differences in TOF values.
- From comparison of catalytic results of both types of reaction and from characterization of vanadium speciation it can be concluded that SBA-15 support is the most suitable structure for deposition of vanadium in the form of isolated monomeric species which are beneficial for C_3-ODH and necessary for C_4-ODH reactions.

Acknowledgements

This work was supported by the Grant Agency of the Czech Republic under project P106/10/0196 and by the University of Pardubice under project SGFChT04.

References

[1] http://www.icis.com/v2/chemicals/9076454/propylene/pricing.html.
[2] O.V. Buyevskaya, M. Baerns, Catal. Today 42 (1998) 315.
[3] F. Cavani, N. Ballarini, A. Cericola, Catal. Today 127 (2007) 113.
[4] E.A. Mamedov, V.C. Corberan, Appl. Catal. A: Gen. 127 (1995) 1.
[5] H.H. Kung, Advances in Catalysis, vol. 40, Academic Press Inc., San Diego, 1994, p. 1.
[6] M.A. Banares, Catal. Today 51 (1999) 319.
[7] R. Grabowski, Catal. Rev. Sci. Eng. 48 (2006) 199.
[8] S. Albonetti, F. Cavani, F. Trifiro, Catal. Rev. Sci. Eng. 38 (1996) 413.
[9] K. Mori, A. Miyamoto, Y. Murakami, J. Phys. Chem. 89 (1985) 4265.
[10] P.K. Rao, K. Narasimha, ACS Symp. Ser. 523 (1993) 231.
[11] T. Blasco, J.M.L. Nieto, Appl. Catal. A: Gen. 157 (1997) 117.
[12] M.L. Pena, A. Dejoz, V. Fornes, E. Rey, M.I. Vazquez, J.M.L. Nieto, Appl. Catal. A: Gen. 209 (2001) 155.
[13] B. Solsona, T. Blasco, J.M.L. Nieto, M.L. Pena, F. Rey, A. Vidal-Moya, J. Catal. 203 (2001) 443.
[14] Y. Wang, Q.H. Zhang, Y. Ohishi, T. Shishido, K. Takehira, Catal. Lett. 72 (2001) 215.
[15] Q.H. Zhang, Y. Wang, Y. Ohishi, T. Shishido, K. Takehira, J. Catal. 202 (2001) 308.
[16] R. Zhou, Y. Cao, S.R. Yan, J.F. Deng, Y.Y. Liao, B.F. Hong, Catal. Lett. 75 (2001) 107.
[17] Y.M. Liu, Y. Cao, N. Yi, W.L. Feng, W.L. Dai, S.R. Yan, H.Y. He, K.N. Fan, J. Catal. 224 (2004) 417.
[18] E.V. Kondratenko, M. Cherian, M. Baerns, D.S. Su, R. Schlogl, X. Wang, I.E. Wachs, J. Catal. 234 (2005) 131.
[19] S. Shylesh, A.P. Singh, J. Catal. 233 (2005) 359.
[20] J. Liu, Z. Zhao, C.M. Xu, A.J. Duan, L. Zhu, X.Z. Wang, Catal. Today 118 (2006) 315.
[21] J.M. Lopez, Top. Catal. 41 (2006) 3.
[22] X.J. Guo, N.H. Xue, S.M. Liu, X.F. Guo, W.P. Ding, W.H. Hou, Microporous Mesoporous Mater. 106 (2007) 246.
[23] P. Knotek, L. Capek, R. Bulanek, J. Adam, Top. Catal. 45 (2007) 51.
[24] E.V. Kondratenko, O. Ovsitser, J. Radnik, M. Schneider, R. Kraehnert, U. Dingerdissen, Appl. Catal. A: Gen. 319 (2007) 98.
[25] W. Liu, S.Y. Lai, H.X. Dai, S.J. Wang, H.Z. Sun, C.T. Au, Catal. Lett. 113 (2007) 147.
[26] T.V.M. Rao, G. Deo, AICHE J. 53 (2007) 1538.
[27] X. Rozanska, R. Fortrie, J. Sauer, J. Phys. Chem. C 111 (2007) 6041.
[28] K. Samson, B. Grzybowska-Swierkosz, Pol. J. Chem. 81 (2007) 1345.
[29] X. Rozanska, J. Sauer, Int. J. Quantum Chem. 108 (2008) 2223.
[30] T. Blasco, P. Concepcion, J.M.L. Nieto, A. Martinez-Arias, Collect. Czech. Chem. Commun. 63 (1998) 1869.
[31] G. Centi, S. Perathoner, F. Trifiro, A. Aboukais, C.F. Aissi, M. Guelton, J. Phys. Chem. 96 (1992) 2617.
[32] G. Bellussi, G. Centi, S. Perathoner, F. Trifiro, ACS Symp. Ser. (1993) 523.
[33] O.V. Buyevskaya, A. Bruckner, E.V. Kondratenko, D. Wolf, M. Baerns, Catal. Today 67 (2001) 369.
[34] S.A. Karakoulia, K.S. Triantafyllidis, G. Tsilomelekis, S. Boghosian, A.A. Lemonidou, Catal. Today 141 (2009) 245.
[35] S.A. Karakoulia, K.S. Triantafyllidis, A.A. Lemonidou, Microporous Mesoporous Mater. 110 (2008) 157.
[36] F. Ying, J.H. Li, C.J. Huang, W.Z. Weng, H.L. Wan, Catal. Lett. 115 (2007) 137.
[37] Y.M. Liu, W.L. Feng, T.C. Li, H.Y. He, W.L. Dai, W. Huang, Y. Cao, K.N. Fan, J. Catal. 239 (2006) 125.
[38] E. Santacesaria, M. Cozzolino, M. Di Serio, A.M. Venezia, R. Tesser, Appl. Catal. A: Gen. 270 (2004) 177.
[39] L. Owens, H.H. Kung, J. Catal. 144 (1993) 202.
[40] Y.M. Liu, Y. Cao, S.R. Yan, W.L. Dai, K.N. Fan, Catal. Lett. 88 (2003) 61.
[41] Y.M. Liu, Y. Cao, K.K. Zhu, S.R. Yan, W.L. Dai, H.Y. He, K.N. Fan, Chem. Commun. (2002) 2832.
[42] M. Setnicka, R. Bulanek, L. Capek, P. Cicmanec, J. Mol. Catal. A 344 (2011) 1.
[43] P.T. Tanev, T.J. Pinnavaia, Science 267 (1995) 865.
[44] T.W. Kim, F. Kleitz, B. Paul, R. Ryoo, J. Am. Chem. Soc. 127 (2005) 7601.
[45] A. Zukal, H. Siklova, J. Cejka, Langmuir 24 (2008) 9837.
[46] D.Y. Zhao, Q.S. Huo, J.L. Feng, B.F. Chmelka, G.D. Stucky, J. Am. Chem. Soc. 120 (1998) 6024.
[47] I.E. Wachs, B.M. Weckhuysen, Appl. Catal. A: Gen. 157 (1997) 67.
[48] G. Centi, Appl. Catal. A: Gen. 147 (1996) 267.
[49] R. Bulanek, L. Capek, M. Setnicka, P. Cicmanec, J. Phys. Chem. C 115 (2011) 12430.
[50] P. Kubelka, F.Z. Munk, Tech. Phys. 12 (1931) 593.
[51] M. Wojdyr, J. Appl. Crystallogr. 43 (2010) 1126.
[52] W.M.H. Sachtler, N.H.D. Boer, Proc. 3rd Int. Congr. Catalysis, Amsterdam, 1964.
[53] C.H. Lee, T.S. Lin, C.Y. Mou, J. Phys. Chem. B 107 (2003) 2543.
[54] S. Shylesh, A.R. Singh, J. Catal. 244 (2006) 52.
[55] L. Capek, J. Adam, T. Grygar, R. Bulanek, L. Vradman, G. Kosova-Kucerova, P. Cicmanec, P. Knotek, Appl. Catal. A: Gen. 342 (2008) 99.
[56] D.E. Keller, T. Visser, F. Soulimani, D.C. Koningsberger, B.M. Weckhuysen, Vib. Spectrosc. 43 (2007) 140.
[57] M. Mathieu, P. Van Der Voort, B.M. Weckhuysen, R.R. Rao, G. Catana, R.A. Schoonheydt, E.F. Vansant, J. Phys. Chem. B 105 (2001) 3393.
[58] J. Tauc, Amorphous and Liquid Semiconductors, Plenum Press, London, 1974.
[59] F. Gao, Y.H. Zhang, H.Q. Wan, Y. Kong, X.C. Wu, L. Dong, B.Q. Li, Y. Chen, Microporous Mesoporous Mater. 110 (2008) 508.
[60] M. Schramlmarth, A. Wokaun, M. Pohl, H.L. Krauss, J. Chem. Soc. Faraday Trans. 87 (1991) 2635.
[61] G. Catana, R.R. Rao, B.M. Weckhuysen, P. Van Der Voort, E. Vansant, R.A. Schoonheydt, J. Phys. Chem. B 102 (1998) 8005.
[62] B.M. Weckhuysen, D.E. Keller, Catal. Today 78 (2003) 25.
[63] B.A. Morrow, A.J. Mcfarlan, J. Non-Cryst. Solids 120 (1990) 61.
[64] C.J. Brinker, R.J. Kirkpatric, D.R. Tallant, B.C. Bunker, B. Montez, J. Non-Cryst. Solids 99 (1988) 418.
[65] E.L. Lee, I.E. Wachs, J. Phys. Chem. C 111 (2007) 14410.
[66] Z. Wu, S. Dai, S.H. Overbury, J. Phys. Chem. C 114 (2010) 412.
[67] J. Dobler, M. Pritzsche, J. Sauer, J. Phys. Chem. C 113 (2009) 12454.
[68] I.E. Wachs, Catal. Today 27 (1996) 437.
[69] N. Das, H. Eckert, H. Hu, I.E. Wachs, J.F. Walzer, F.J. Feher, J. Phys. Chem. 97 (1993) 8240.
[70] P. Gruene, T. Wolfram, K. Pelzer, R. Schlogl, A. Trunschke, Catal. Today 157 (2010) 137.
[71] J. Santamaria-Gonzalez, J. Luque-Zambrana, J. Merida-Robles, P. Maireles-Torres, E. Rodriguez-Castellon, A. Jimenez-Lopez, Catal. Lett. 68 (2000) 67.
[72] H. Berndt, A. Martin, A. Bruckner, E. Schreier, D. Muller, H. Kosslick, G.U. Wolf, B. Lucke, J. Catal. 191 (2000) 384.
[73] G. Du, S. Lim, M. Pinault, C. Wang, F. Fang, L. Pfefferle, G.L. Haller, J. Catal. 253 (2008) 74.
[74] G. Martra, F. Arena, S. Coluccia, F. Frusteri, A. Parmaliana, Catal. Today 63 (2000) 197.
[75] M.M. Koranne, J.G. Goodwin, G. Marcelin, J. Catal. 148 (1994) 369.
[76] P. Kustrowski, Y. Segura, L. Chmielarz, J. Surman, R. Dziembaj, P. Cool, E.F. Vansant, Catal. Today 114 (2006) 307.
[77] F. Arena, F. Frusteri, A. Parmaliana, Appl. Catal. A: Gen. 176 (1999) 189.
[78] J.M. Kanervo, M.E. Harlin, A.O.I. Krause, M.A. Banares, Catal. Today 78 (2003) 171.
[79] M.A. Banares, J.H. Cardoso, F. Agullo-Rueda, J.M. Correa-Bueno, J.L.G. Fierro, Catal. Lett. 64 (2000) 191.
[80] M.V. Martinez-Huerta, J.L.G. Fierro, M.A. Banares, Catal. Commun. 11 (2009) 15.
[81] M.V. Martinez-Huerta, X. Gao, H. Tian, I.E. Wachs, J.L.G. Fierro, M.A. Banares, Catal. Today 118 (2006) 279.
[82] G. Grubert, J. Rathousky, G. Schulz-Ekloff, M. Wark, A. Zukal, Microporous Mesoporous Mater. 22 (1998) 225.